Measurement of nonlinear optical coefficients of zinc cobalt ferrite using the z-scan technique with variable intensity

F Habibi[1], M Moradi[1, 2, *], and N Davoodian[1]

1. Department of Physics, University of Shahrekord, Shahrekord, Iran
2. Photonic Research Group, University of Shahrekord, Shahrekord, Iran
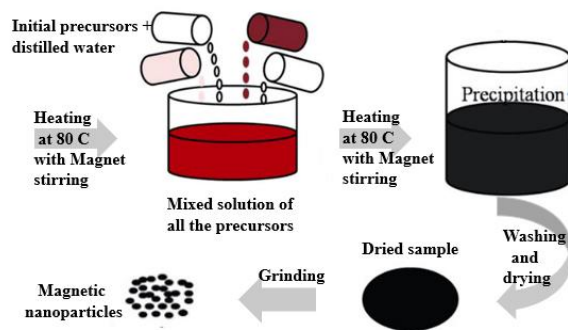
Email: moradi@sku.ac.ir

Abstract

In this study, cobalt zinc ferrite nanoparticles were synthesized with the formula $Co_{x-1}Zn_xFe_2O_4$ using a Co-precipitation method, varying x values. A green laser was utilized as the excitation source to measure the nonlinear refractive index and absorption coefficient at three different intensities. The z-scan method was employed for both closed and open apertures at room temperature. The findings indicate that as the initial laser intensity increases, the nonlinear refractive index and nonlinear absorption coefficient decrease. Additionally, an increase in concentration at a specific intensity results in a limited appearance of nonlinear properties. Furthermore, an increase in the linear absorption coefficient corresponds to an increase in these nonlinear coefficients. This nanostructure proves valuable for night sensing applications due to its negative refractive index under strong nonlinearity. In this context, the spinel model of the nanostructure holds promising potential for 6G communication applications.

Keywords: nanoparticles, zinc cobalt ferrite, z-scan method, nonlinear refractive index, nonlinear absorption index

1. Introduction

The investigation of the nonlinear optical properties of nanoparticles in colloidal solutions is an active area of research with numerous potential applications, including optical signal processing and devices for optical communication [1-4]. The outcomes of nanoscience are translated into nanotechnology, leading to the development of new materials and functional capabilities. Currently, nanophysics is emerging as a significant and expanding branch of nanoscience [5]. Metallic nanoparticles often exhibit unique and significantly altered physical, chemical, and biological properties in comparison to their macro-scaled counterparts, primarily due to their high surface-to-volume ratio. As a result, substantial research has been conducted on these nanoparticles in recent years [6, 7]. Metallic nanoparticles possess properties that are influenced by their size and shape, making them valuable for a range of applications including catalysis, sensing, optics, antibacterial activity, and data storage [8, 9]. There are two main routes for preparing metal nanoparticles. The first is a physical approach employing methods such as evaporation/condensation and laser ablation. The second is a chemical approach involving the reduction of metal ions in a solution under conditions conducive to the subsequent formation of small metal clusters or aggregations [10]. The z-scan method is a technique used for determining nonlinear refraction and absorption, and it is widely employed in material characterization because it provides information on both the sign and magnitudes of the real and imaginary parts of nonlinear susceptibility [11-15]. A significant portion of the documented characterizations of nonlinearities in nanoparticles within dielectric materials involved the utilization of lasers with wavelengths near the absorption maximum of the surface Plasmon resonance of the nanoparticles [16]. However, in this current study, we employed a green laser beam to investigate the impact of The investigation of the nonlinear optical properties of nanoparticles in colloidal solutions is an active area of research with numerous potential applications, including optical signal processing and devices for optical communication [1-4]. The outcomes of nanoscience are translated into nanotechnology, leading to the development of new materials and functional capabilities. Currently, nanophysics is emerging as a significant and expanding branch of nanoscience [5]. Metallic nanoparticles often exhibit unique and significantly altered physical, chemical, and biological properties in comparison to their macro-scaled counterparts, primarily due to their high surface-to-volume ratio. As a result, substantial research has been conducted on these nanoparticles in recent years [6, 7].

Figure 1. The schematic scheme of co-precipitation method.

Metallic nanoparticles possess properties that are influenced by their size and shape, making them valuable for a range of applications including catalysis, sensing, optics, antibacterial activity, and data storage [8, 9]. There are two main routes for preparing metal nanoparticles. The first is a physical approach employing methods such as evaporation/condensation and laser ablation. The second is a chemical approach involving the reduction of metal ions in a solution under conditions conducive to the subsequent formation of small metal clusters or aggregations [10]. The z-scan method is a technique used for determining nonlinear refraction and absorption, and it is widely employed in material characterization because it provides information on both the sign and magnitudes of the real and imaginary parts of nonlinear susceptibility [11-15]. A significant portion of the documented characterizations of nonlinearities in nanoparticles within dielectric materials involved the utilization of lasers with wavelengths near the absorption maximum of the surface Plasmon resonance of the nanoparticles [16]. However, in this current study, we employed a green laser beam to investigate the impact of particles on the nonlinearity properties of cobalt zinc ferrite solution. The measurements were conducted for both closed and open aperture configurations.

2. Experiments

For the co-preparation of cobalt zinc ferrite nanoparticles, various laboratory equipment was employed, including three 500 or 10000 joules volumetric flasks, a 1-liter volumetric flask, a 250cc graduated cylinder, two one or two-liter magnets to ensure solution uniformity, a digital scale for precise weighing of raw materials, and a magnetic stirrer heater (utilized for both heating and achieving uniform solutions).

Additionally, a thermometer was utilized to monitor the temperature of solutions on the heater, and a pipette was used for precise separation of specific solution quantities. The co-preparation method is illustrated in figure 1.

The X-Ray Diffraction device (XRD) was employed to determine the average diameters of cobalt zinc ferrite nanoparticles, revealing a measurement of 11.5 nm for $Co_{0.8}Zn_{0.2}Fe_2O_4$. Figure 2 displays the results of the X-ray diffraction pattern of the samples. Analysis of the X-ray diffraction pattern results, using X'Pert software, indicates that the identified peaks in the diffraction

patterns align with reference cards 00-022-1086, 00-022-1012, and 00-003-0864. It is observed that as zinc increases and cobalt decreases in the crystalline structure of the ferrite, the peaks become broader. Considering that the ionic radius of zinc is larger than the ionic radius of cobalt, by substituting Zn instead of Co, the smaller ion gives its place to the smaller ion and causes the network to expand. This expansion increases the lattice parameter and the distance between the plates, and we expect the X-ray diffraction peaks to shift to smaller angles, which we can see in the figures if we compare the peaks of the cards with the peaks of the sample. The main peak is located at higher angles of Zn cards and at smaller angles of co cards, which indicates the difference in the size of cobalt and zinc ions. Considering the larger ionic radius of zinc compared to cobalt, the substitution of Zn for Co results in the smaller ion taking the place of the larger one, leading to an expansion of the network. This expansion increases the lattice parameter and the distance between the plates. Consequently, we anticipate a shift in the X-ray diffraction peaks towards smaller angles. This shift is observable when comparing the peaks of the reference cards with those of the sample in the figures. The primary peak is positioned at higher angles in Zn cards and at smaller angles in Co cards, indicating the disparity in size between cobalt and zinc ions. The separation between the plates is determined by utilizing the (311) peak, characterized by the highest intensity in the X-ray diffraction pattern, and applying the Bragg relationship ($n\lambda = 2d\sin(\theta)$). For determining the lattice parameter, we employ the equation ($a = d\sqrt{h^2 + k^2 + l^2}$), where k, h, and l represent Miller indices, and d is the distance between the plates [17]. Additionally, the average size of the crystals is computed using the equation ($d = \kappa\lambda/\beta\cos(\theta)$), with θ, λ, β, and κ denoting the Bragg angle, wavelength, full width at half maximum, and Scherrer constant (0.9 for spherical particles), respectively. The outcomes of these measurements are presented in table (1).

As the substitution of zinc for cobalt increases, there is a reduction in the average size of the crystals. Additionally, a higher lattice parameter corresponds to an increased distance between the plates. Consequently, in accordance with Bragg's law, the angles of the peaks decrease as the distance between the plates increases. Moreover, a reduction in the size of the crystal leads to a broader peak width in the X-ray diffraction pattern. As the percentage of Zn in the solution increases, there is a decrease in the average size of the crystals. In such instances, a larger lattice parameter corresponds to an increased d value. As the d parameter increases, in accordance with Bragg's law, the peaks exhibit a decrease in size. Additionally, a reduction in crystal size results in a broader peak width in the X-ray diffraction pattern. Upon analysis of the results, it becomes evident that the samples are at the nanoscale, and their crystal structure is identified as cubic spinel. Figure 3 illustrates the chemical structure of three types of ferrite (ZnFe₂O₄, Co Fe₂O₄ and $Co_{1-x}Zn_xFe_2O_4$).
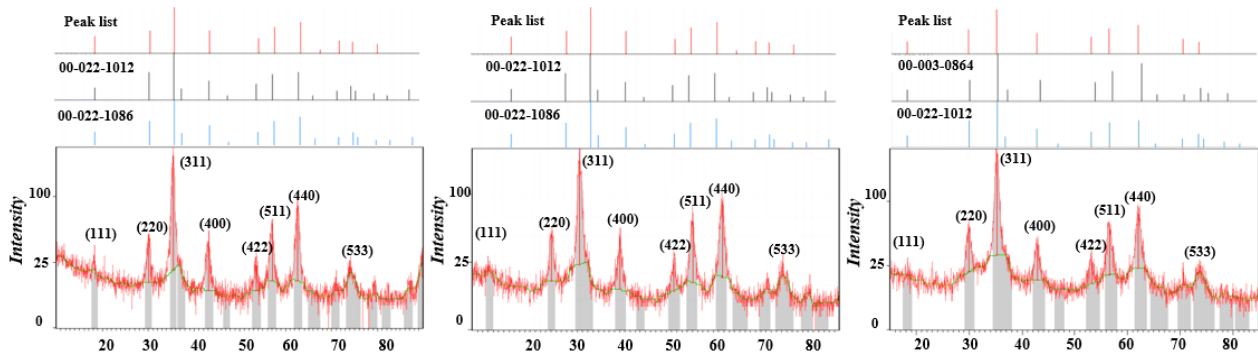
Figure 2. Match the results of X-ray diffraction pattern and reference cards.

Table 1. The results of X-ray diffraction pattern

Samples	d (Å)	$\boldsymbol{a}$ (Å)	D (nm)
$Co_{0.8}Zn_{0.2}Fe_2O_4$	2.529	8.388	11.5
$Co_{0.6}Zn_{0.4}Fe_2O_4$	2.536	8.410	8.7
$Zn\ Fe_2O_4$	2.545	8.441	8.6
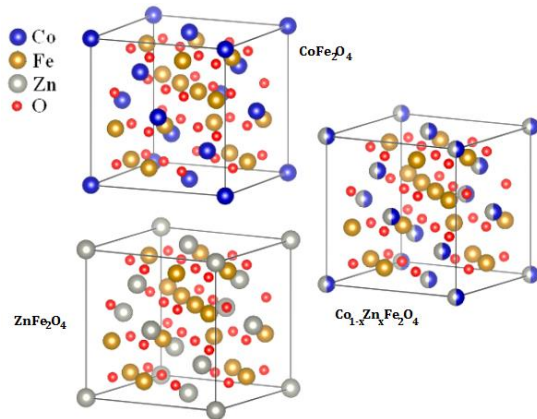
Figure 3. Cubic structure of $Co_{1-x}Zn_xFe_2O_4$, $ZnFe_2O_4$ and $CoFe_2O_4$ [17].

Figure 2 depicts the M-H diagrams of the samples at room temperature, obtained using the AGFM. On the right side of the image, transmission electron microscope (TEM) images for the sample are presented. The images reveal an average particle size of approximately 11 nm for $Co_{0.8}Zn_{0.2}Fe_2O_4$. Notably, the samples did not attain magnetic saturation even at the maximum applied field of kOe9, possibly attributable to the nanoparticle size.

To assess nonlinear properties, a single-beam z-scan method employing closed and open aperture configurations was employed to determine the nonlinear refractive and nonlinear absorption coefficients. The nonlinear refraction was extracted by moving the sample through the focal point, and the nonlinear transmission was measured as a function of the sample position, with an aperture positioned at the far field.

Figure 5 illustrates the schematic representation of a single-beam z-scan experiment, employing closed and open aperture setups to determine the nonlinear refractive and nonlinear absorption coefficients. The experiments utilized a 532 nm laser beam generated by a Nd-YAG laser. The beam was focused to a small spot through a lens, and the sample underwent z-axis movement via a motorized translational stage.
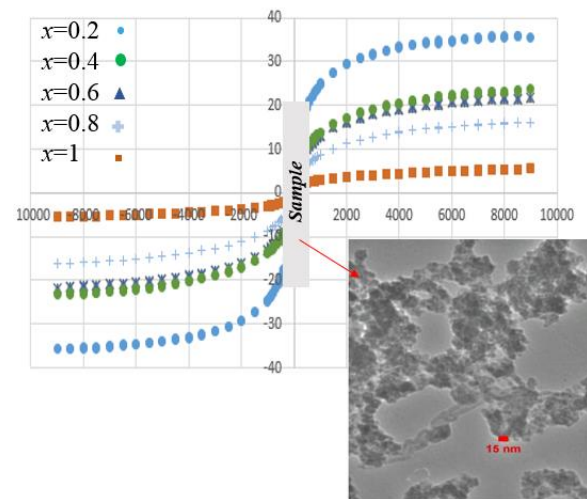

Figure 4. The diagram of M-H samples, the TEM images of $Co_{0.8}Zn_{0.2}Fe_2O_4$ sample (at the right).

The transmitted light in the far field traversed through the aperture, and the detector recorded the beam intensity. The assessment of the nonlinear refractive index and absorption coefficient of ferrite solutions was conducted using various apertures (open and closed) for intensities I_1, I_2, and I_3, corresponding to values of (232.6 w/cm², 2558.9 w/cm², and 5117.8 w/cm²).

3. Closed z-scan experiment

The closed aperture z-scan configuration is illustrated in figure 4. Experimental data is depicted by circle symbols, and theoretical fits to the closed aperture z-scan equations are represented by solid lines. The nonlinear refractive index of the nanoparticle was determined using the straightforward relationship proposed by Sheikh-Bahaei [18]

$$n_2 = \frac{\Delta\varphi_0\lambda}{2\pi I_0 L_{eff}} \ , \tag{1}$$

In these expressions, λ represents the wavelength of the laser light, I_0 is the peak intensity within the sample, $\Delta\varphi_0$ is the nonlinear phase shift, and Leff is the effective thickness, as defined by the following relations [18, 19]

$$\Delta T_{p-v} = 0.406\left(1-S\right)^{0.25}\Delta\varphi_0 \ , \tag{2}$$

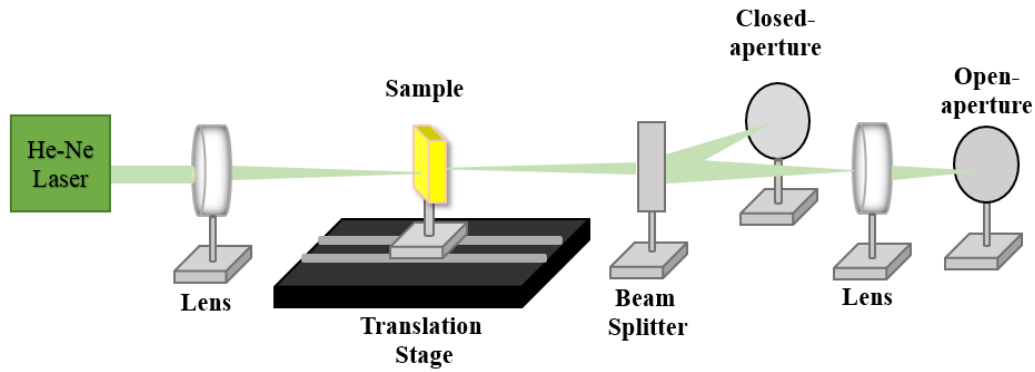$$L_{eff} = \left[1-\exp(-\alpha_0 L)\right]/\alpha_0 \ , \tag{3}$$

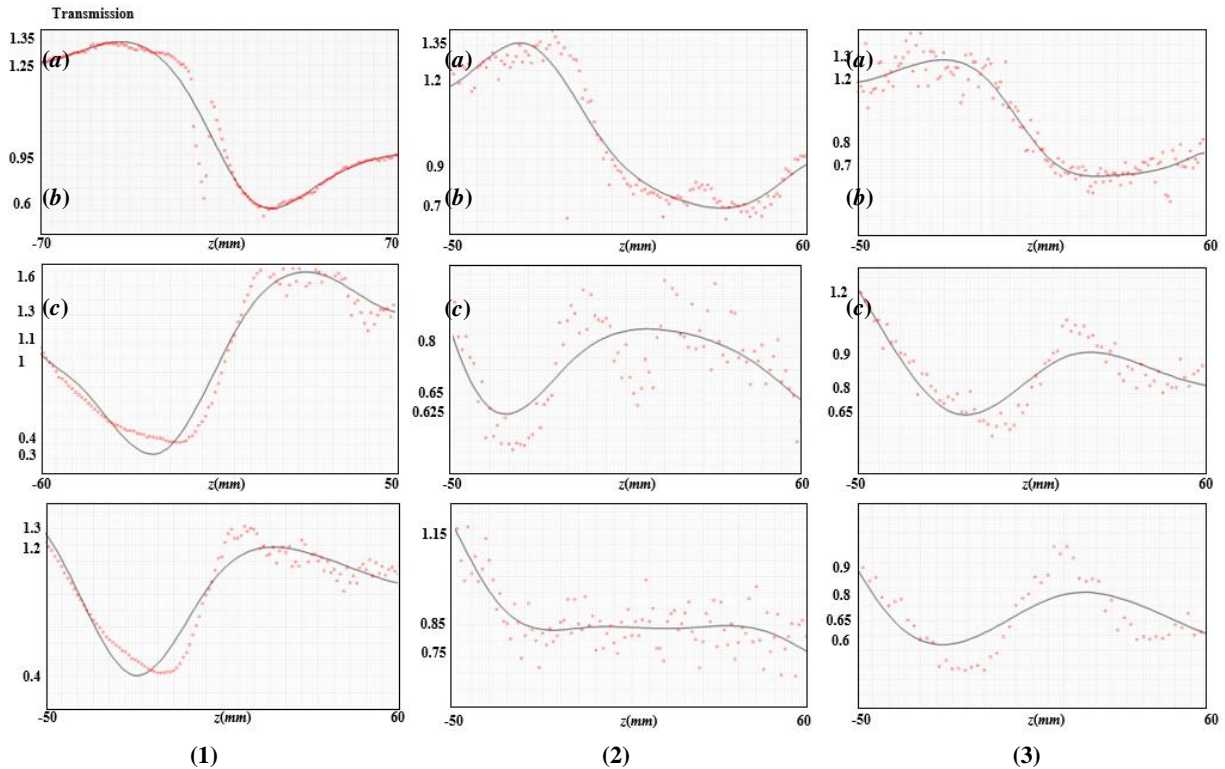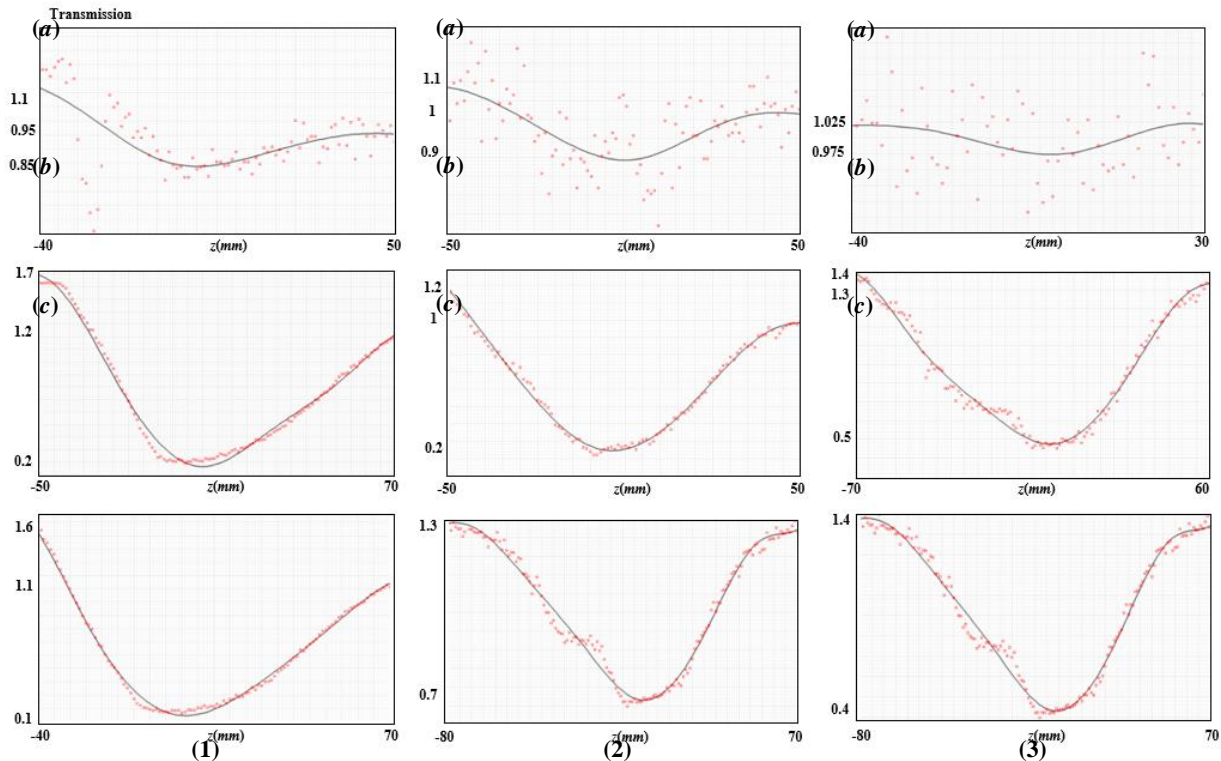**Figure 5**. The schematic scheme of z-scan technique.

Figure 6. Normalized diagrams of closed apertures of 1) $Co_{0.8}Zn_{0.2}Fe_2O_4$, 2) $Co_{0.6}Zn_{0.4}Fe_2O_4$ and 3) $Co_{0.4}Zn_{0.6}Fe_2O_4$ for different intensities a) 232.6w/cm^2, b) 2558.9 w/cm^2 and c) 5117.8 w/cm^2 .

In this context, S represents the aperture linear transmittance, L is the thickness of the sample, and α is the linear absorption coefficient at the wavelength λ.

Figure 6 displays both the experimental (red pattern) and fitted (black line) transmission profiles for the closed aperture using the equation 2, aiming to ascertain the nonlinear refractive index under various x values and intensities. In the presented graphs, at moderate intensities (2558.9 w/cm²) and high intensities (5117.8 w/cm²), the sequence of observations reveals a valley followed by a peak. Conversely, at low intensities (232.6 w/cm²), the sequence is characterized by a peak followed by a valley. When the outcome initially features a valley followed by a peak, the nonlinear refractive index is positive. However, in cases where the

peak is followed by the valley, the nonlinear refractive index is negative. This implies that the material exhibits diverging lens-like behavior, leading to self-divergence. The calculated values for the nonlinear refractive index (n₂) of the current samples are presented and listed in table 2. As we mentioned before and displayed in figure (3), Zinc cobalt ferrites are spinel ferrites and are known for exhibiting unique electromagnetic properties, including negative refractive index behavior under specific conditions. This phenomenon, known as negative refraction, occurs due to the unique electromagnetic properties of ferrites, specifically their ability to exhibit both magnetic and dielectric responses simultaneously.

Figure 7. Normalized diagrams of open apertures of 1) $Co_{0.8}Zn_{0.2}Fe_2O_4$, 2) $Co_{0.6}Zn_{0.4}Fe_2O_4$ and 3) $Co_{0.4}Zn_{0.6}Fe_2O_4$ for different intensities a) 232.6 w/cm², b) 2558.9 w/cm² and c) 5117.8 w/cm².

Table 2. The nonlinear refractive indexes [n_1 (I_1), n_2 (I_2) and n_2 (I_2)] of Zinc cobalt ferrite solution for intensities I_1 (232.6 w/cm²), I_2 (2558.9 w/cm²) and I_3 (2558.9 w/cm²).

Samples	n_2 (w/cm²) $\times 10^{-7}$	n_2 (w/cm²) $\times 10^{-7}$	n_2 (w/cm²) $\times 10^{-7}$
$Co_{0.8}Zn_{0.2}Fe_2O_4$	-4.545	1.021	0.629
$Co_{0.6}Zn_{0.4}Fe_2O_4$	-5.117	1.446	0.406
$Co_{0.4}Zn_{0.6}Fe_2O_4$	-4.607	1.032	0.601

4. Open z-scan experiment

The illustration in figure 7 depicts the open aperture z-scan. The symbols correspond to experimental data, while the solid lines represent theoretical fits to the open aperture z-scan equations. The nonlinear absorption coefficient β (cm/w) can be determined through fitting the experimental data of the open aperture measurement using the established equation utilized by [18]

$$T(z) = \frac{\ln[1 + \beta I_0 L_{eff} / 1 + (z/z_0)^2]}{\beta I_0 L_{eff} / 1 + (z/z_0)^2}, \qquad (4)$$

Here $T(z)$ represents the normalized transmission for the open aperture. Figure 7 illustrates Transmission diagrams of the open aperture for three intensities. The open aperture graphs at low intensity (232.6 w/cm²) show shallower depths compared to medium (2558.9 w/cm²) and high (5117.8 w/cm²) intensities for all solutions. Additionally, at low intensities, there are more scattering points, and the graphs exhibit a greater minimum at the intensity's lowest point. To ascertain nonlinear absorption in the uniaxial scanning apparatus, a converging lens is employed in lieu of an aperture to ensure all incident light reaches the detector.

5. Effect of linear absorption coefficient on nonlinear coefficients

In this section, we illustrate the variations of the nonlinear refractive index and the nonlinear absorption coefficient by changing the linear absorption coefficient. Figures (8-1) to (8-3) depict the details of these changes.

By examining figure 8, it becomes evident that the nonlinear coefficients increase in tandem with the rise in the linear absorption coefficient as the intensity varies. These variations align with the equation $\alpha(I) = \alpha_0 + \beta I$ [21, 22]. The linear absorption coefficient affects the nonlinear refractive index and nonlinear absorption coefficient due to their interplay in the material's response to intense light. Essentially, the linear absorption coefficient influences the material's initial absorption of light, which in turn affects the population of excited states and the subsequent nonlinear optical processes like self-phase modulation and two-photon absorption. So, a higher linear absorption coefficient can lead to stronger nonlinear effects due to increased population of excited states, affecting both the nonlinear refractive index and the nonlinear absorption coefficient.
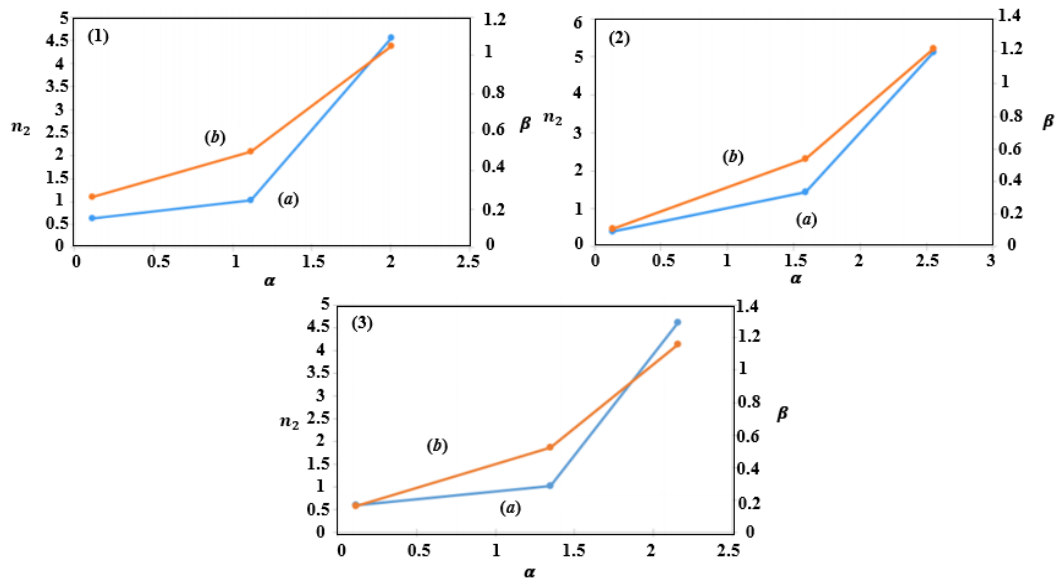
Figure 8. Changes in (a) the nonlinear refractive index and (b) the nonlinear absorption coefficient of the solution in terms of the linear absorption coefficient for 1) $Co_{0.8}Zn_{0.2}Fe_2O_4$, 2) $Co_{0.6}Zn_{0.4}Fe_2O_4$ and 3) $Co_{0.4}Zn_{0.6}Fe_2O_4$.

Table 3. The effect of concentration on nonlinear coefficients for intensity of 2558.9 w/cm^2.

Concentration (gr/lit)	Co Fe₂O₄		Co₀.₈Zn₀.₂Fe₂O₄		Co₀.₆Zn₀.₄ Fe₂O₄	
	n_2 (w/cm²)×10⁻⁷	β(cm/w)	n_2 (w/cm²)×10⁻⁷	β(cm/w)	n_2 (w/cm²)×10⁻⁷	β(cm/w)
1.6	0.975	0.4	1.021	0.501	1.466	0.537
3.2	0.473	0.372	0.213	0.16	0.729	0.199
4.8	0.368	0.236	0.201	0.158	0.221	0.082

Changing concentration for both closed and open aperture Now, we investigate the impact of concentration on the nonlinear refractive index and nonlinear absorption coefficient, keeping

the laser intensity constant as a parameter. The experiments were conducted for three materials with different x, and the outcomes of these measurements are presented in table 3. Analysis of Recessional Velocity Distribution from a Terrestrial Perspective

As observed, an increase in the concentration of cobalt ferrite solution results in a decrease in both the nonlinear absorption coefficient and nonlinear refractive index. With the elevated concentration, there is a reduction in the separation between peaks and valleys in the obtained graphs, indicating an anticipated decrease in the nonlinear coefficients. It is because increasing the concentration can reduce the density of absorption centers within the material. This means there are fewer sites available for nonlinear absorption processes to occur, leading to a decrease in the nonlinear absorption coefficient. Furthermore, the reason behind the decrease of nonlinear refractive index with the increase of ferrite concentration

is the change of its susceptibility in nonlinear optical processes.

6. Conclusion

The nonlinear refractive index (n_2) and nonlinear absorption coefficients (β) of ferrite nanoparticles were accurately determined. Changes in the nonlinear coefficients were observed with increasing concentration. Notably, the nonlinear refractive index exhibited a negative sign at lower initial intensities. As the zinc percentage rises in the zinc-cobalt ferrite solution, the nonlinear coefficients initially show an increase followed by a decrease for low and medium intensities. The maximum nonlinear coefficients are observed when the zinc and cobalt percentages are nearly equal. However, this trend reverses at high intensities. Higher initial laser intensity is associated with a decrease in the nonlinear coefficients. Additionally, an increase in concentration corresponds to a decrease in the nonlinear coefficients. Moreover, an elevation in the linear absorption coefficient contributes to an increase in both nonlinear coefficients.

References

1. R R A Ganeev, et al., *Tech. Phys.* **47** (2002) 991.
2. T Jia, et al., *Opt. Laser. Technol*. **40** (2008) 936.
3. K H Cho, et al., *Electrochim. Acta*. **51** (2005) 956.
4. J F Wang, et al., *Science* **24** (2001) 1455.
5. G Sergeev and T Shabatina, *Colloids Surf. A: Physicochem. Eng. Aspects* **313** (2008) 18.
6. V Sharma, R Yngard, and Y Lin, *Adv. Colloid Interface Sci*. **145** (2009) 83.
7. H Huang and Y Yang, *Compos. Sci. Technol*. **68** (2008) 2948.
8. Y Choi, N H Ho, and C H Tung, *Angew. Chem. Int. Ed*, **46** (2007) 707.

9.   A Vilchis-Nestor, et al., *Mater. Lett*. **62** (2008) 3103.
10. M Oliveira, et al., *J. Colloid Interface Sci*. **292** (2005) 429.
11. G Yang, et al., *Opt. Mater*. **25** (2004) 439.
12. T Catunda, J P Andreeta, and J C Castro, *Appl. Opt*. **25** (1986) 2391.
13. S L Guo, et al., *Opt. Quant. Electron*. **35** (2003) 693.
14. H Tingchao, et al., *J. Modern. Opt*. **372** (2008) 3937.
15. G S He, et al., *Appl. Phys*. **81** (1997) 2529.
16. G S He, et al., *IEEE J. Quantum Electron*. **39** (2003) 1003.
17. A Johan, et al., *J. Phys. Conf. Ser*. **1282** (2019) 012032.
18. M Sheikh-Bahaei, A A Said, and E W Van Stryland, *Opt. Lett*. **14** (1989) 955.
19. M Sheikh-Bahaei, et al., *IEEE J. Quantum Electron*. **26** (1990) 760.
20. M H Majlesara, Z Javadi, and R S Sirohi, *Optik*. **122** (2011) 1961.
21. H Zhang, et al., *Opt. Lett*. **11** (2012) 1856.
22. R W Boyd, A L Gaeta, and E Giese, "*Nonlinear optics. In Springer Handbook of Atomic, Molecular, and Optical Physics*", Springer International Publishing, Cham, Switzerland, (2008).